# Exposure of Monomolecular Lithographic Patterns to Ambient: An X-ray Photoemission Spectromicroscopy Study

**C.-H. Chen,*,† M.-L. Huang,† S.-C. Wang,† R. Klauser,† A. Shaporenko,‡ and M. Zharnikov*,‡**

*National Synchrotron Radiation Research Center, 101 Hsin-Ann Road, Hsinchu 30076, Taiwan, and Angewandte Physikalische Chemie, Universität Heidelberg, 69120 Heidelberg, Germany*

*Received: June 17, 2006; In Final Form: July 13, 2006*

Patterned self-assembled monolayers (SAMs) of alkanethiolates (AT) on Au and Ag substrates were imaged and characterized by scanning photoelectron microscopy (SPEM). The patterns were prepared in situ by direct writing with the zone-plate-focused X-ray beam provided by the SPEM station. Whereas both AT/Au and AT/Ag behaved alike upon the irradiation, which resulted in similar contrasts in the fabricated patterns and similar microspot spectra from the irradiated areas, the intensity relationship between the patterned and nonpatterned areas changed by different pathways for the Au and Ag substrates after the exposure of the patterns to ambient. The SPEM data imply that weakly bound molecular fragments are desorbed from the irradiated areas upon air exposure in the case of Ag, whereas adsorption of airborne molecules from ambient occurs for the Au substrate. The origin of the observed differences is presumably related to the specific branching patterns of irradiation-induced modification of AT/Au and AT/Ag.

## 1. Introduction

Technological progress in frontier areas of modern industry relies upon the development of new approaches for micro- and nanofabrication and patterning. In this context, perspective resist and template materials are monomolecular films—self-assembled monolayers (SAMs), which are well-ordered and densely packed 2D-ensembles of chainlike organic molecules anchored to a substrate by a suitable headgroup.[1−5] The patterning of SAMs or with SAMs can be performed in different ways, including microcontact printing,[6,7] ultraviolet interferometric lithography,[8] dip-pen lithography,[7,9] scanning tunneling microscopy,[10,11] atomic force microscopy,[12,13] etc. Also, SAMs can be patterned down to the nanometer length scale by electron or X-ray irradiation, using either proximity printing geometry or a focused beam.[14−17] The character and extent of electron- and X-ray-induced modification of SAMs depend on both architecture of the SAM constituents and their exact arrangement in the film.[17] By using an advanced molecular design, these parameters can be precisely adjusted in view of a specific application. In particular, depending on the character of the SAM constituents, SAMs can serve as both positive and negative resists for conventional patterning or as a template for chemical lithography.[14,15,17] The respective properties are valid for both e-beam and X-ray lithography, since the major impact of X-ray irradiation is provided by photoelectrons and inelastic secondary electrons.[17,18]

The precise adjustment of the properties of a SAM resist relies upon a detailed knowledge of the physical and chemical changes occurring at the exposure of SAMs to electrons and X-ray photons. Such knowledge is predominantly gained by different spectroscopies, including infrared-reflection absorption spectroscopy,[17] X-ray photoelectron spectroscopy,[17−20] X-ray absorption spectroscopy,[17,20] mass spectroscopy,[21−23] and some other spectroscopic techniques. Also, the respective spectromicroscopies, providing direct "chemical" access to SAM-based lithographic patterns, can be quite useful, as, e.g., was demonstrated by the example of X-ray photoelectron microscopy[24−26] and X-ray absorption microscopy.[27] An especially versatile experimental tool is synchrotron-based scanning photoelectron microscopy (SPEM), which can be simultaneously used for the fabrication and spectroscopic characterization of SAM-based lithographic patterns.[28,29] This technique was successfully applied for the patterning of different aliphatic and aromatic SAMs and characterization of the fabricated patterns without their exposure to ambient, i.e., in situ.[28,29] It is, however, well-known that the exposure of such patterns to ambient might result in their further modification. In particular, alkanethiolate (AT) SAMs on Au, which are the common positive SAM resist, exhibit a pronounced increase in their thickness upon exposure to ambient after irradiation.[24,25] This was explained by the adsorption of airborne carbon-containing molecules onto the SAM−ambient interface, which becomes quite rough and chemically reactive in the course of electron or X-ray irradiation.[24,25] The enhanced reactivity and roughness of this interface is associated with such irradiation-induced processes as the stochastic cleavage of the individual chemical bonds within the SAM, desorption of hydrocarbon fragments, and loss of orientational and conformational order.[17,30]

In the present study, we intended to visualize and study the effect of the exposure to ambient in detail, taking AT SAMs on Au and Ag as test systems and using a SPEM setup for the fabrication and characterization of the respective lithographic patterns. Note that AT/Au and AT/Ag exhibit similar bulk densities, but different 2D lattices, lateral densities (higher for AT/Ag), and molecular inclinations (smaller for AT/Ag).[2,4,31] Also, the S−Ag bond is presumably stronger than the S−Au one.[31−35] In particular, the former bond was found to be much more stable under irradiation than the latter one, so that the mostly intact SAM−substrate interface was persistent in irradi-

* Address correspondence to these authors. E-mail:chchen@nsrrc.org.tw and michael.zharnikov@urz.uni-heidelberg.de.
† National Synchrotron Radiation Research Center.
‡ Universität Heidelberg.

10.1021/jp063779t CCC: $33.50 
Published on Web 08/22/2006

ated AT/Ag, but not in AT/Au.[35] Furthermore, the orientational and conformational order in AT/Ag persists longer in the course of irradiation than in AT/Au.[35] In contrast, the extent of the irradiation-induced desorption of hydrocarbon species was found to be very similar for AT/Au and AT/Ag.[35]

In the following section we describe the experimental procedure and techniques. The results are presented and briefly discussed in section 3. An extended analysis of the data is given in section 4 followed by a summary in section 5.

## 2. Experimental Section

The gold and silver substrates were prepared by thermal evaporation of 200 nm of gold or 100 nm of silver (99.99% purity) onto mica or polished single-crystal silicon (100) wafers (Silicon Sense) primed with a 5 nm titanium adhesion layer. The AT compounds of this study were dodecanthiol, $CH_3(CH_2)_{11}$-SH abbreviated as C12, and hexadecanethiol, $CH_3(CH_2)_{15}SH$ abbreviated as C16. The compounds were purchased from Sigma Aldrich and used without purification. The SAMs were formed by immersion of the substrates in a 1 mmol solution of C12 and C16 in ethanol. After immersion, the samples were carefully rinsed with pure ethanol, blown dry with argon, and shipped to the experimental station in argon-filled glass containers.

The fabrication and characterization of the SAM patterns was performed at the SPEM station located at the U5 undulator beamline of the National Synchrotron Radiation Research Center (NSRRC) in Hsinchu, Taiwan.[24] The spatial resolution of the setup is about 100 nm. The station is equipped with Fresnel zone plate optics, which provides a focused X-ray beam, and a 16 channel hemispherical electron energy analyzer, which enables a simultaneous acquisition of 16 images at different binding energies during the raster-scanning of the sample. The respective stack of images is thus representative for a definite range of binding energies (BEs) in the vicinity of the characteristic emissions. Such stacks were collected for the Au 4f, Ag 3d, and C1s BE ranges. The photon energy was set at either 380 eV for the Au 4f and C1s imaging or at 480 eV for the Ag 3d imaging. Due to the individual adjustment of the SPEM setup for every sample and every photon energy the energy scales of the respective microspot spectra for the different samples can be slightly shifted with respect to each other. However, every set of the microspot spectra contained a characteristic emission ($Au4f_{7/2}$, $Ag3d_{5/2}$, or C1s for the pristine C12/Au and C12/Ag),[36−38] which could be used for the individual calibration of the absolute BE scale.

Since we were mostly interested in possible changes of the lithographic patterns after their exposure to ambient, we fabricated the simplest square pattern ($10 \times 10\ \mu m^2$). The parameters of the focusing optics of the SPEM setup were kept the same for the writing and imaging and only the settings of the pixel width and dwell time were different. For the pattern fabrication, an exposure time of 80 ms and a pixel width of 200 nm have been chosen while the imaging of the patterned surface was performed with a dwell time of 30 ms and a pixel width of 300 nm, i.e., at about an order of magnitude smaller X-ray exposure as compared to the writing. The imaging was performed both in situ, immediately after the pattern fabrication, and ex situ, after a prolonged (for several days) exposure of the patterns to ambient. By integrating over selected areas ($25 \times 25$ pixel$^2$ squares) of the collected images, the 16-point C1s, Au 4f, and Ag 3d XPS microspot spectra were derived for both pristine and irradiated regions of the SAM patterns.

In addition to the SPEM experiments, we monitored the change in the macroscopic wetting properties of AT SAMs in the course of electron and X-ray irradiation by measuring their water contact angles. The respective experiments were performed on the C16 SAMs on Au and Ag. These films were homogeneously irradiated with 10 eV electrons, which are representative for the secondary electrons, playing the major role in the X-ray-induced damage.[17,18] The electrons were provided by a flood gun. Advancing contact angles of Millipore water were measured with a Krüss goniometer Model G1. The measurements were performed under ambient conditions with the needle tip in contact with the drop. At least three measurements at different locations on each sample were made. The averaged values are reported. Deviations from the average were less than $\pm 1°$.

## 3. Results

In Figure 1a,b we present in situ Au4f (1a) and C1s (1b) microspot spectra related to the areas inside (circles, solid line) and outside (triangles, dashed line) of the $10 \times 10\ \mu m^2$ square patterned in the C12 resist on Au, along with the respective SPEM images corresponding to channel 11 for the Au4f spectra and channels 10 and 12 for the C1s spectra. As seen in these figures, the Au4f microspot spectra from the irradiated area have a higher intensity as compared to the pristine film, which correlates with the respective SPEM image at the BE position of the $Au4f_{7/2}$ emission, in which the irradiated area exhibits a stronger emission signal. Taking into account that this signal is attenuated by the C12 film, this behavior highlights irradiation-induced desorption of the SAM constituents and their fragments within the irradiated area. Such a desorption is accompanied by chemical changes in the residual film, as suggested by the downward shift (from ~284.9 to ~284.4 eV) and broadening of the C1s peak in the respective microspot spectra from the patterned square as compared to those from the outside pristine areas. These changes correlate with the contrast of the irradiated area in the respective SPEM images. They can be associated with the dehydrogenation, chemical heterogenization, and structural disordering of the irradiated C12 film (clear evidence for these processes was provided, in particular, by near edge X-ray absorption fine structure spectroscopy and microspectroscopy at the C K-edge).[17,20,27] Also the amplitude of the C1s peak related to the irradiated area is lower than that of the analogous emission stemming from the pristine areas, which agrees with the opposite behavior of the Au 4f signal and supports our conclusion about the irradiation-induced desorption.

C12/Ag exhibits a similar behavior as C12/Au as far as the imaging is performed in situ. The respective data are presented in Figure 2. They include in situ Ag3d (2a) and C1s (2b) microspot spectra related to the areas inside (circles, solid line) and outside (triangles, dashed line) of the $10 \times 10\ \mu m^2$ patterned square in C12 resist on Ag, along with the respective SPEM images corresponding to channel 12 for the Ag3d spectra and channels 10 and 12 for the C1s spectra. The observed difference between the microspot spectra of the irradiated and pristine areas as well as the contrast of the SPEM images mimics those of the C12/Au pattern in Figure 1, even though the BE positions of the C1s emission for pristine C12/Au and C12/Ag are different, 284.9 and 285.2 eV, respectively.[37,38] We can, thus, conclude that the irradiation of C12/Ag, similar to C12/Au, results in desorption of the SAM constituents and their fragments, as well as in dehydrogenation, chemical heterogenization, and structural disordering of the residual films.

The exposure of the lithographic patterns to ambient (referred to below as ex situ patterns) resulted in their pronounced modification. The respective microspot spectra and SPEM

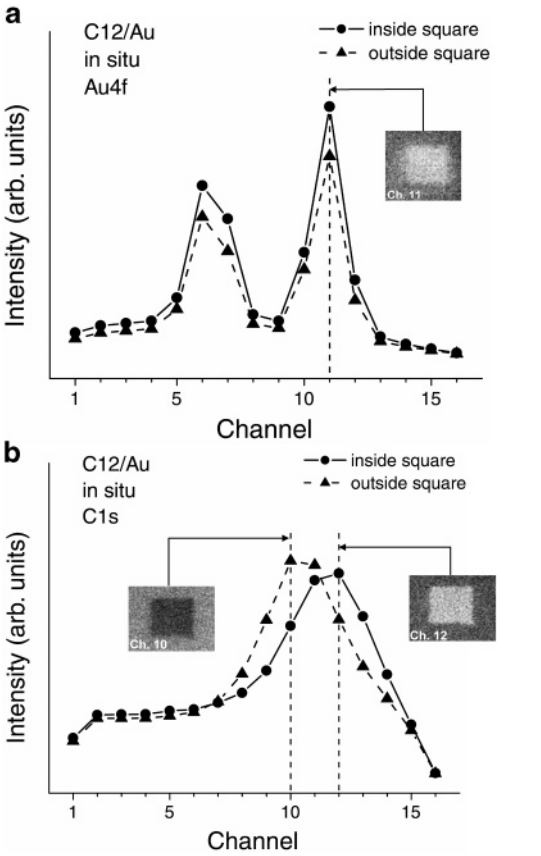


**Figure 1.** In situ Au4f (a) and C1s (b) microspot spectra related to the areas inside (circles, solid line) and outside (triangles, dashed line) of the $10 \times 10$ $\mu m^2$ square pattern in the C12 resist on Au, along with the respective SPEM images corresponding to channel 11 for the Au4f spectra and channels 10 and 12 for the C1s spectra. The microspot spectra were derived from a stack of 16 successive SPEM images. With increasing channel number, the binding energy decreases in steps of about 0.75 and 0.375 eV for Au4f and C1s, respectively. The BE position of the C1s emission for pristine C12/Au is 284.9 eV.[37,38]

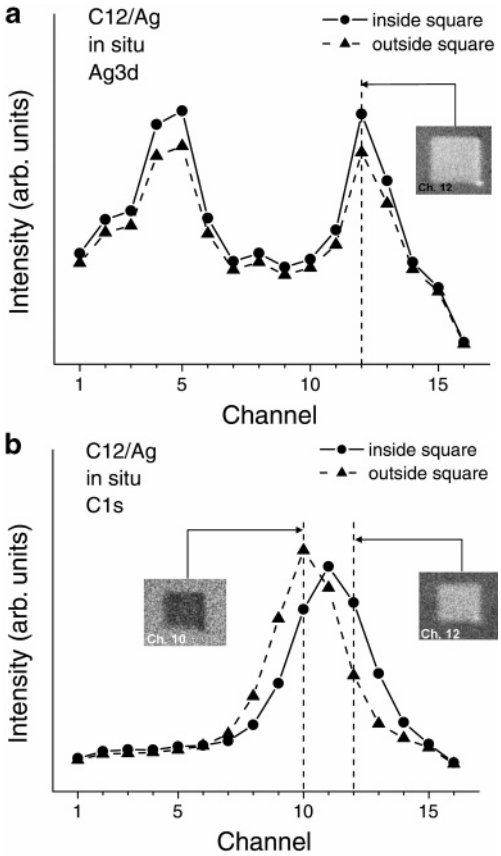


**Figure 2.** In situ Ag3d (a) and C1s (b) microspot spectra related to the areas inside (circles, solid line) and outside (triangles, dashed line) of the $10 \times 10$ $\mu m^2$ square pattern in the C12 resist on Ag, along with the respective SPEM images corresponding to the channel 12 for the Ag3d spectra and channels 10 and 12 for the C1s spectra. The microspot spectra were derived from a stack of 16 successive SPEM images. With increasing channel number, the binding energy decreases in steps of about 0.75 and 0.375 eV for Ag3d and C1s, respectively. The BE position of the C1s emission for pristine C12/Ag is 285.2 eV.[37,38]

images are presented in Figures 3 (C12/Au) and 4 (C12/Ag) and arranged in a similar way as those in Figures 1 and 2. For C12/Au, the $Au4f_{7/2}$ SPEM image in Figure 3a exhibits an opposite contrast as compared to the analogous image in Figure 1a. The respective $Au4f_{7/2}$ microspot spectra behave accordingly. As compared to the pristine areas, Au4f peaks for the irradiated areas exhibited a higher signal before the exposure to ambient (Figure 1a) and a lower signal after this exposure (Figure 3a). This suggests the adsorption of airborne molecules onto the irradiated areas of C12/Au upon exposure to ambient, in accordance with previous observations.[24−26] This conclusion is supported by the C1s microspot spectra and C1s SPEM image related to the maximum of the C1s peak in Figure 3b, which exhibit a higher C1s signal from the irradiated areas as compared to the pristine ones. Note that this intensity relationship is exactly opposite to that observed before the air exposure (Figure 1b). However, in addition to the inversion of the C1s intensity relationship between the irradiated and pristine areas, air exposure of the irradiated area resulted in the shift of the C1s peak back to the BE position characteristic of the pristine C12 film, as shown in Figure 3b.

Despite all the similarity of the in situ patterns, ex situ patterns for C12/Au and C12/Ag are quite different. As seen from the comparison of Figures 2a and 4a, for C12/Ag, there are no contrast and intensity relationship inversions in the Ag3d SPEM images and microspot spectra, respectively; the signal from the irradiated area was and remains noticeably higher. C1s SPEM images and respective microspectra in Figures 2b and 4b behave accordingly: the irradiated areas exhibit a lower signal than the pristine ones both before and after the exposure to ambient, with the difference being even larger than for the respective in situ images and microspot spectra. However, there is a similar backward energy shift of the C1s peak in the C1s microspot spectra of the ex situ C12/Ag pattern (Figure 4b) as was observed for the case of C12/Au (Figure 3b).

## 4. Discussion

The in situ spectromicroscopic and microspectroscopic characterization of monomolecular lithographic patterns written by a focused X-ray beam in AT (C12) resist on Au and Ag suggests a similar character of the irradiation-induced processes for both substrates. The irradiated areas exhibited a higher signal from the substrate and a lower signal from the monomolecular resist, which was associated with irradiation-induced desorption of the SAM constituents and their fragments, in accordance with previous results, showing a similar extent of the respective process in AT SAMs on Au and Ag.[17,35] For both C12/Au and C12/Ag, a broadening and shift of the C1s peak by about −0.4 eV were observed, which, taking into account the results of previous studies,[17,27,35,39] was related to irradiation-induced dehydrogenation, disordering, and chemical heterogenization of the residual film.

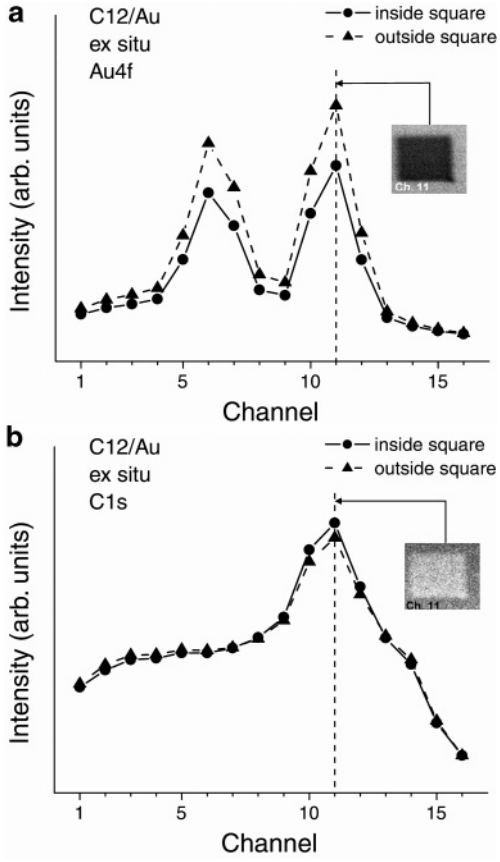


**Figure 3.** Ex situ Au4f (a) and C1s (b) microspot spectra related to the areas inside (circles, solid line) and outside (triangles, dashed line) of the $10 \times 10\ \mu m^2$ square pattern in the C12 resist on Au, along with the respective SPEM images corresponding to channel 11 for both Au4f and C1s spectra. The microspot spectra were derived from a stack of 16 successive SPEM images. With increasing channel number, the binding energy decreases in steps of about 0.75 eV for both Au4f and C1s. The BE position of the C1s emission for pristine C12/Au is 284.9 eV.[37,38]

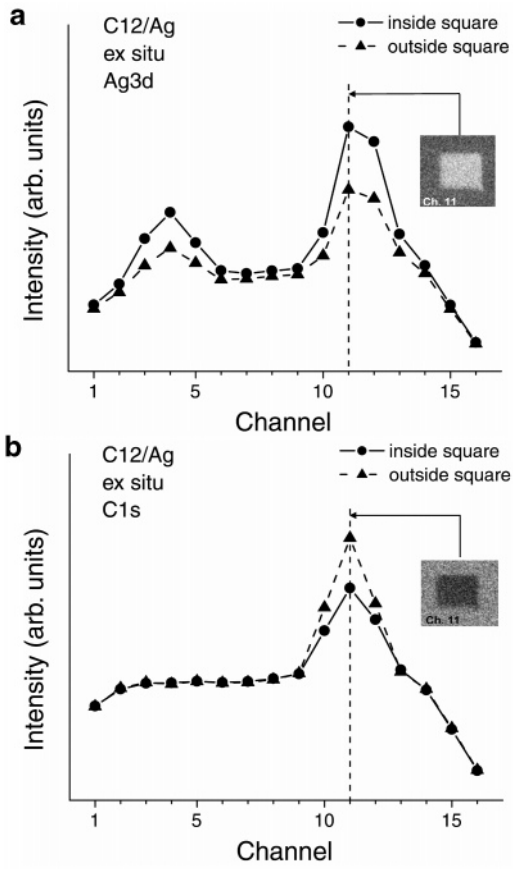


**Figure 4.** Ex situ Ag3d (a) and C1s (b) microspot spectra related to the areas inside (circles, solid line) and outside (triangles, dashed line) of the $10 \times 10\ \mu m^2$ square pattern in the C12 resist on Ag, along with the respective SPEM images corresponding to channel 11 for both Ag3d and C1s spectra. The microspot spectra were derived from a stack of 16 successive SPEM images. With increasing channel number, the binding energy decreases in steps of about 0.75 eV for both Ag3d and C1s. The BE position of the C1s emission for pristine C12/Ag is 285.2 eV.[37,38]

However, these presumably very similar lithographic patterns behaved quite differently upon their prolonged exposure to ambient. Whereas for the ex situ C12/Au pattern SPEM image contrast and signal intensity relationship between the irradiated and pristine areas were inverted as compared to the in situ pattern, their parameters were mostly unaffected by the exposure to ambient in the case of C12/Ag. Moreover, for the latter pattern, the signal difference between the irradiated and pristine areas becames even larger after their exposure to ambient. Apart from this difference, the behavior of the C12/Au pattern can only be explained by the adsorption of airborne molecules onto the irradiated areas, in agreement with previous observations.[24−26] It can be assumed that the irradiation creates chemically active sites and nonsaturated bonds at the SAM−ambient interface that can provide docking sites for the airborne molecules. Considering a significant increase in the C1s signal from the irradiated areas of the C12/Au pattern and appearance of only a weak O1s signal (equivalent to 0.3 ML of $CO/CO_2$ upon an extensive irradiation),[17] the dominant species among the adsorbed airborne molecules are presumably hydrocarbons, e.g. methane, which is present in air in a significant amount. The bonding of these species to the SAM−ambient interface (=SAM surface) should be sufficiently strong to survive the sample handling and pressure reduction upon the transfer from ambient to ultrahigh vacuum of the SPEM station, and, thus, this is presumably a chemisorption.

In contrast to C12/Au, there was no noticeable adsorption of airborne molecules onto the irradiated areas upon the exposure of the C12/Ag pattern to ambient. Moreover, it seems that a part of the irradiated film desorbed. The desorption probably involved hydrocarbon fragments in the vicinity of the SAM−ambient interface, which were only weakly bound to the residual film.

The difference between the C12 patterns on Au and Ag can only be related to different chemical composition and reactivity of the respective SAM−ambient interfaces after the extensive irradiation. To probe the macroscopic properties of these interfaces, we performed measurements of advancing and receding water contact angles for an AT (C16) SAM on Au and Ag as functions of irradiation dose. The respective results are presented in Figure 5. As shown in this figure, the contact angles of C16/Au and C16/Ag decrease smoothly in the course of irradiation, with the extent of decrease being identical for both systems. Also, the contact angle hysteresis changes identically for both C16/Au and C16/Ag, starting from about 10° for the pristine films and slightly increasing during the irradiation, suggesting that the roughness of the SAM/ambient interface was not that strongly affected by X-ray irradiation, as has been assumed before.[17,30] On the basis of all these results, we can conclude that the macroscopic wetting properties of irradiated alkanethiolate SAMs on Au and Ag are quite similar

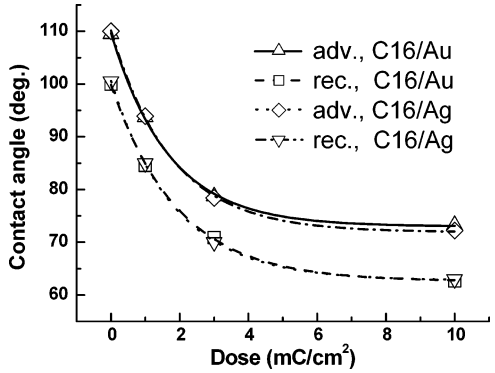


**Figure 5.** Advancing (up triangles and diamonds) and receding (squares and down triangles) water contact angles for C16/Au (up triangles and squares) and C16/Ag (diamonds and down triangles) as functions of irradiation dose.

and cannot explain the observed difference in the reactivity of the respective lithographic patterns toward airborne molecules.

The only explanation that is left to us is the difference in the exact branching patterns of electron- and X-ray-induced modification of AT SAMs on Au and Ag. According to our previous results,[35] whereas the extent of irradiation-induced desorption in both systems is similar, the orientational and conformational order in AT/Ag persists significantly longer in the course of irradiation than in AT/Au, and the thiolate−silver bond is much more stable under irradiation than the thiolate−gold one. Thus, irradiated AT/Ag has a more intact, SAM-like character than completely disordered AT/Au, in which the residuals of the aliphatic matrix are intermixed with dialkylsulfide species, appearing after the cleavage of the thiolate−gold bonds at the SAM−substrate interface and subsequent diffusion of released fragments into the film.[39] It is not clear at the moment why these quite subtle differences influence the reactivity of the SAM−ambient interface to such a significant extent. The effect is, however, obvious.

Another interesting and unexpected finding is the backward shift of the C 1s emission from the irradiated areas upon the exposure of the X-ray microbeam patterns to ambient. Whereas for both C12/Au and C12/Ag a shift of the C1s peak by about −0.4 eV upon an extensive irradiation was observed (in situ), the respective BE position changed back to the value characteristic of the pristine films after the exposure to ambient (ex situ), as seen in the microspot spectra in Figures 3b and 4b. It looks, thus, that the exposure to ambient results in chemical changes or/and a reorganization of the residual molecules and molecular fragments in the irradiated areas. Note that the BE position of the C1s emission in AT SAMs cannot be exclusively related to their chemical composition, but also to the interfacial dipole, because of a specific pinning of their Fermi and vacuum levels to the Fermi level of the spectrometer.[40,41] In particular, such a pinning can explain the difference in the BE position of the C1s emission between AT/Au and AT/Ag,[40,41] although there exists an alternative explanation, involving antiscreening of the photoemission hole in an aliphatic chain by the neighboring molecules.[38]

## 5. Conclusion

In summary, using synchrotron-based X-ray photoelectron microscopy, we observed pronounced substrate effects in the chemical activity of monomolecular lithographic patterns upon their exposure to ambient. Whereas the surface of extensively irradiated alkanethiolate SAMs on Au is found to be reactive toward airborne hydrocarbon species, resulting in their adsorption, the surface of the analogous films on Ag remains mostly inert, and even desorption of weakly bound hydrocarbon fragments occurs. Since the macroscopic wetting properties of both surfaces were found almost identical, their different reactivities toward airborne molecules were explained by microscopic differences in the exact organization and chemical composition of the irradiation-modified films. In particular, irradiated AT SAMs on Ag have a more intact, SAM-like character as compared to the completely disordered SAMs on Au, in which the residuals of the aliphatic matrix are intermixed with dialkylsulfide species, appearing after the extensive damage of the SAM−substrate interface. The exact mechanism behind the different reactivities of both systems is, however, not clear at the moment, and further experiments, above all HRXPS, can be helpful to clarify this issue.

In addition, independent of the substrate, the exposure to ambient was found to cause chemical changes and a reorganization of the residual molecules and molecular fragments in the irradiated areas of AT SAMs.

The presented data show that X-ray photoelectron microscopy can be successfully applied to visualize and characterize monomolecular lithographic patterns. As compared to optical microscopy, this technique provides a direct "chemical" access to the visualized objects. As compared to spectroscopy, specromicroscopy and microspectroscopy allow direct comparison of intensity and microspot spectra from different areas, excluding an ambiguity related to a precise calibration of the individual spectra for different samples.

**Acknowledgment.** M.Z. and A.S. thank M. Grunze (Universität Heidelberg) for the support of this work and J.-D. Liao (NCKU, Tainan) for the cooperation at NSRRC. Assistance from the NSRRC staff is acknowledged. The work was supported by the German BMBF (05KS4VHA/4), DFG (ZH 63/9-2), and a DAAD/NSC grant 423/rc-PPP-sr.

## References and Notes

(1) Ulman, A. *An Introduction to Ultrathin Organic Films*: *Langmuir−Blodgett to Self-Assembly*; Academic Press: New York, 1991.
(2) Ulman, A. *Chem. Rev.* **1996**, *96*, 1533.
(3) Ulman, A., Ed. *Thin films*: *self-assembled monolayers of thiols*; Academic Press: San Diego, CA, 1998.
(4) Schreiber, F. *Prog. Surf. Sci.* **2000**, *65*, 151.
(5) Love, J. C.; Estroff, L. A.; Kriebel, J. K.; Nuzzo, R. G.; Whitesides, G. M. *Chem. Rev.* **2005** *105*, 1103.
(6) Kumar, A.; Biebuyck, H. A.; Whitesides, G. M. *Langmuir* **1994**, *10*, 1498.
(7) Gates, B. D.; Xu, Q.; Stewart, M.; Ryan, D.; Willson, C. G.; Whitesides, G. M. *Chem. Rev.* **2005**, *105*, 1171.
(8) Kim, S. O.; Solak, H. H.; Stoykovich, M. P.; Ferrier, N. J.; de Pablo, J. J.; Nealey, P. F. *Nature* **2003**, *424*, 411.
(9) Piner, R. D.; Zhu, J.; Xu, F.; Hong, S.; Mirkin, C. A. *Science* **1999**, *283*, 661.
(10) Xu, S.; Liu, G. *Langmuir* **1997**, *13*, 127.
(11) Fuierer, R. R.; Carroll, R. L.; Feldheim, D. L.; Gorman, C. B. *Adv. Mater.* **2002**, *14*, 154.
(12) Maoz, R.; Cohen, S. R.; Sagiv, J. *Adv. Mater.* **1999**, *11*, 55.
(13) Maoz, R.; Cohen, S. R.; Sagiv, J. *Adv. Mater.* **2000**, *12*, 725.
(14) Geyer, W.; Stadler, V.; Eck, W.; Zharnikov, M.; Gölzhäuser, A.; Grunze, M. *Appl. Phys. Lett.* **1999**, *75*, 2401.
(15) Eck, W.; Stadler, V.; Geyer, W.; Zharnikov, M.; Gölzhäuser, A.; Grunze, M. *Adv. Mater.* **2000**, *12*, 805.
(16) Gölzhäuser, A.; Geyer, W.; Stadler, V.; Eck, W.; Grunze, M.; Edinger, K.; Weimann, Th.; Hinze, P. *J. Vac. Sci. Technol. B* **2000**, *18*, 3414.
(17) Zharnikov, M.; Grunze, M. *J. Vac. Sci. Technol. B* **2002**, *20*, 1793 and references therein.
(18) Laibinis, P. E.; Graham, R. L.; Biebuyck, H. A.; Whitesides, G. M. *Science* **1991**, *254*, 981.
(19) Wirde, M.; Gelius, U.; Dunbar, T.; Allara, D. L. *Nuc. Instrum. Methods Phys. Res., Sect. B* **1997**, *131*, 245.

(20) Jäger, B.; Schürmann, H.; Müller, H. U.; Himmel, H. J.; Neumann, M.; Grunze, M.; Wöll, Ch. *Z. Phys. Chem.* **1997**, *202*, 263.
(21) Olsen, C.; Rowntree, P. A. *J. Chem. Phys.* **1998**, *108*, 3750.
(22) Huels, M. A.; Dugal, P. C.; Sanche, L. *J. Chem. Phys.* **2003**, *118*, 11168.
(23) Feulner, P.; Niedermayer, T.; Eberle, K.; Schneider, R.; Menzel, D.; Baumer, A.; Schmich, E.; Shaporenko, A.; Tai, Y.; Zharnikov, M. *Phys. Rev. Lett.* **2004**, *93*, 178302.
(24) Klauser, R.; Hong, I.-H.; Lee, T.-H.; Yin, G.-C.; Wei, D.-H.; Tsang, K.-L.; Chuang, T. J.; Wang, S.-C.; Gwo, S.; Zharnikov, M.; Liao, J.-D. *Surf. Rev. Lett.* **2002**, *9*, 213.
(25) Klauser, R.; Zharnikov, M.; Hong, I.-H.; Wang, S.-C.; Gölzhäuser, A.; Chuang, T. J. *J. Phys. IV* **2003**, *104*, 459.
(26) Klauser, R.; Hong, I.-H.; Wang, S.-C.; Zharnikov, M.; Paul, A.; Gölzhäuser, A.; Terfort, A.; Chuang, T. J. *J. Phys. Chem. B* **2003**, *107*, 13133.
(27) Zharnikov, M.; Shaporenko, A.; Paul, A.; Gölzhäuser, A.; Scholl, A. *J. Phys. Chem. B* **2005**, *109*, 5168.
(28) Klauser, R.; Huang, M.-L.; Wang, S.-C.; Chen, C.-H.; Chuang, T. J.; Terfort, A.; Zharnikov, M. *Langmuir* **2004**, *20*, 2050.
(29) Klauser, R.; Chen, C.-H.; Huang, M.-L.; Wang, S.-C.; Chuang, T. J.; Zharnikov, M. *J. Electron Spectrosc. Relat. Phenom.* **2005**, *144*−*147*, 393.
(30) Müller, H. U.; Zharnikov, M.; Völkel, B.; Schertel, A.; Harder, P.; Grunze, M. *J. Phys. Chem. B* **1998**, *102*, 7949.
(31) Laibinis, P. E.; Whitesides, G. M.; Allara, D. L.; Tao, Y.-T.; Parikh, A. N.; Nuzzo, R. G. *J. Am. Chem. Soc.* **1991**, *113*, 7152.
(32) Walczak, M. M.; Chung, C.; Stole, S. M.; Widrig, C. A.; Porter, M. D. *J. Am. Chem. Soc.* **1991**, *113*, 2370.
(33) Jaffey, D. M.; Madix, R. J. *Surf. Sci.* **1994**, *311*, 159.
(34) Chenakin, S. P.; Heinz, B.; Morgner, H. *Surf. Sci.* **1999**, *421*, 337.
(35) Zharnikov, M.; Frey, S.; Heister, K.; Grunze, M. *Langmuir* **2000**, *16*, 2697.
(36) Moulder, J. F.; Stickle, W. E.; Sobol, P. E.; Bomben, K. D. *Handbook of X-ray Photoelectron Spectroscopy*; Chastian, J., Ed.; Perkin-Elmer Corp.: Eden Prairie, MN, 1992.
(37) Heister, K.; Zharnikov, M.; Grunze, M.; Johansson, L. S. O. *J. Phys. Chem. B* **2001**, *105*, 4058.
(38) Heister, K.; Johansson, L. S. O.; Grunze, M.; Zharnikov, M. *Surf. Sci.* **2003**, *529*, 36.
(39) Heister, K.; Zharnikov, M.; Grunze, M.; Johansson, L. S. O.; Ulman, A. *Langmuir* **2001**, *17*, 8.
(40) Tarlov, M. J. *Langmuir* **1992**, *8*, 80.
(41) Ahn, H.; Zharnikov, M.; Whitten, J. E. *Chem. Phys. Lett.* **2006**, in press.